Adsorption (2011) 17: 453–460
DOI 10.1007/s10450-010-9282-6

Activation and structural and adsorption features of activated carbons with highly developed micro-, meso- and macroporosity

V.M. Gun'ko · V.V. Turov · O.P. Kozynchenko · V.G. Nikolaev · S.R. Tennison · S.T. Meikle · E.A. Snezhkova · A.S. Sidorenko · F. Ehrburger-Dolle · I. Morfin · D.O. Klymchuk · S.V. Mikhalovsky

Received: 11 August 2010 / Accepted: 14 October 2010 / Published online: 30 October 2010

Abstract Three sets of activated carbons (ACs) were prepared with the same precursor but activated differently (by CO_2 or water vapour) with various burn-off levels. The ACs demonstrate increased deviation of the pore shape from the slitshaped model with increasing burn-off and contributions of pores of different sizes depending on the activation type. Significant re-arrangement of adsorption complexes, especially of the Van der Waals type characteristic for nonpolar or weakly polar adsorbates (H_2, CH_4, CH_2Cl_2, $CHCl_3$), occurs in both micropores and mesopores of ACs with decreasing temperature. The behaviour of their mixtures with water and DMSO can strongly differ from that of individual adsorbates.

Keywords Activated carbons · CO_2 activation · H_2O activation · Structural characteristics · Particle morphology · Interfacial behaviour

1 Introduction

Activated carbons (ACs) as the most effective adsorbents are characterised by high porosity ($V_p = 1$–2 cm^3/g) and large specific surface area ($S_{BET} = 1000$–3000 m^2/g) (Bansal et al. 1988; Smisek and Cerny 1970; Gregg and Sing 1982; Marsh et al. 1997). The adsorption properties of ACs depend strongly on their structural features, especially contributions of micro- (pore half-width $x < 1$ nm), meso- ($1 < x < 25$ nm) and macropores ($x > 25$ nm), as well as on the number and type of surface functionalities containing H, O, N, P, S and other atoms (Juárez-Galán et al. 2009; Lenghaus et al. 2002; Molina-Sabio and Rodríguez-Reinoso 2004). These structural features affect other properties of the materials used, e.g., as catalysts (Rodríguez-Reinoso 1998; Ahumada et al. 2002; Bansal et al. 1988). Contributions of pores of different sizes can be varied on both controlled carbonisation of precursors and subsequent activation depending on the type of activating agents (CO_2, water vapour, basic and acidic compounds, etc.), temperature, pressure, flow velocity, and burn-off level (Rodríguez-Reinoso et al. 1995, 2000a, 2000b; Marsh et al. 1997; Molina-Sabio et al. 1995, 1996; Molina-Sabio and Rodríguez-Reinoso 2004; Bansal et al. 1988). For many purposes, ACs with maximal porosity up to $V_p = 2.5 - 3.0$ cm^3/g, but without loss of particle integrity, and S_{BET} up to 3000–4000 m^2/g are of a special interest because such great structural characteristics allow one

Electronic supplementary material The online version of this article (doi:10.1007/s10450-010-9282-6) contains supplementary material, which is available to authorized users.

V.M. Gun'ko · S.T. Meikle · S.V. Mikhalovsky (✉)
School of Pharmacy & Biomolecular Sciences, University of Brighton, Brighton BN2 4GJ, UK
e-mail: s.mikhalovsky@brighton.ac.uk

V.M. Gun'ko · V.V. Turov
Chuiko Institute of Surface Chemistry, 17 General Naumov Street, 03164 Kiev, Ukraine

O.P. Kozynchenko · S.R. Tennison
MAST Carbon International Ltd., Henley Park, Guildford, Surrey, GU3 2AF, UK

V.G. Nikolaev · E.A. Snezhkova · A.S. Sidorenko
Kavetsky Institute of Experimental Pathology, Oncology and Radiobiology, 45 Vasilkovskaya Str., 03194 Kiev, Ukraine

F. Ehrburger-Dolle · I. Morfin
Laboratoire de Spectrométrie Physique, UMR 5588 CNRS—UJF, 38402 Saint Martin d'Hères Cedex, France

D.O. Klymchuk
Kholodny Institute of Botany, 2 Tereschenkivska Street, 01601 Kiev, Ukraine

to use the materials for effective gas storage, fast and complete removal of toxic compounds from gases and liquids, etc. (Rodriguez-Reinoso 2006; Marsh et al. 1997; Bansal et al. 1988; Silvestre-Albero et al. 2010). Superactivated carbon materials gained special importance in medicine, particularly, in the problem of removal of strongly protein-bound toxins and proinflammatory cytokines from whole blood and blood plasma (Sarnatskaya et al. 2002, 2007). However, certain regularities in the structure-property relationships for activated and superactivated carbons need additional investigations. Therefore, the aim of this work was to produce and characterise ACs, possessing great V_p (>2 cm^3/g) and S_{BET} (3000–3400 m^2/g) values, broad pore size distributions (PSD) with significant contributions of micro-, meso- and macropores, and keeping integrity of granules after high-level burn-off under activation with CO_2 and water vapour, in comparison with ACs with lower burn-off. Analysis of the behaviour of a mixture of adsorbates of different polarity in confined space of micro- and mesopores of ACs is another aim of the work carried out using low-temperature ^{1}H NMR spectroscopy. This behaviour is of importance for practical applications of carbon adsorbents for storage of H_2 or CH_4, removal of organic pollutants from gaseous and liquid (e.g. aqueous) flows, as well as for medical purposes, especially extracorporeal blood purification.

2 Materials and methods

Small porous phenol formaldehyde resin beads (Tennison et al. 2004) were carbonised in a CO_2 flow to 1073 K at a ramp rate of 3 K/min (sample labelled as C-0). Additional activation by CO_2 at 1183 K and different residence times results from 25% (C-25) to 86% (C-86) burn-off. This is the first series of ACs with carbon particles of 0.15–0.50 mm in size characterised by high specific surface area, porosity and adsorption capacity (Tennison et al. 2004; Gun'ko et al. 2008a, 2008b). The second and third sets of ACs were prepared using the C-0 sample as initial one activated by water vapour in a fixed bed reactor, similar to that used on activation by CO_2 (labelled Wf-x, x = 24–77% burn-off) and in a fluidised bed reactor at 1020–1050 K (labelled W-x, x = 42.5–88.3% burn-off at bulk density 0.18–0.10 g/cm^3, respectively).

The structural characteristics of carbon samples were determined using the nitrogen adsorption-desorption isotherms recorded at 77.4 K using a Micromeritics Gemini or ASAP 2010 adsorption analysers. The pore size distributions (PSDs) were calculated using the DFT method (Do et al. 2001) with a regularisation procedure based on the CONTIN algorithm (Provencher 1982; Gun'ko and Do 2001; Gun'ko and Mikhalovsky 2004; Gun'ko et al. 2008a, 2008b). The differential PSDs with respect to pore volume (PSD_V, $f_V(x) \sim dV/dx$, $\int f_V(x)dx \sim V_p$) and specific surface area (PSD_S, $f_S(x) \sim dS/dx$, $\int f_S(x)dx \sim S$) were shown as incremental ones (IPSD, $\sum \Phi_{V,i}(x) = V_p$, $\sum \Phi_{S,i}(x) = S$). The differential $f_S(x)$ functions were used to estimate the deviation (Δw) of the pore shape from the model of slitshaped pores (Gun'ko and Mikhalovsky 2004). Additionally, to show a complex pore shape of maximum activated carbons, the model with a mixture of slitshaped and cylindrical pores and voids between nanoparticles was applied with self-consisting regularization allowing determination of contributions of pores of different types (Gun'ko 2000). Non-local DFT, NLDFT (with the model of siltshaped/cylindrical pores) and quenched solid DFT, QSDFT (slitshaped pore model) (Quantachrome software, version 2.02) were used to compute the PSDs of ACs.

Small angle X-ray scattering (SAXS) measurements were performed on the French CRG beamline D2AM at the European Synchrotron Radiation Facility (ESRF), Grenoble, France. The PSD functions were calculated from the SAXS data using the integral equation described in detail elsewhere (Pujari et al. 2007). The chord size distributions as a geometrical statistic description of a solid phase in ACs were also calculated from the SAXS data (Dieudonné et al. 2000).

Adsorption of H_2O, H_2, CH_4, CH_2Cl_2, $CHCl_3$, $(CH_3)_2SO$, and $CDCl_3$ (Aldrich, $C_D \geq 99.5\%$) and certain their mixtures onto C-30 (selected as a representative carbon sample with main contribution of narrow pores) was studied using low-temperature (190–280 K) ^{1}H NMR method as described in detail elsewhere (Gun'ko et al. 2005). Notice that this technique can be also used to determine the structural characteristics of carbons (Krutyeva et al. 2009; Gun'ko et al. 2005).

3 Results and discussion

An increase in the carbon activation by CO_2 to 86% burn-off leads to parallel enhancement of contribution of micro- and mesopores to the pore volume (Table 1, V_{mic} and V_{mes}, Fig. 1). However, the contribution of the mesopores to the specific surface area is significant only for ACs at a high level of the activation, when the S_{mic}/S_{BET} value decreases (Fig. 1). A reason of these changes in the structural characteristics is clearly visible in Fig. 2 showing the appearance of a peak of narrow mesopores at $1 < x < 2$ nm for C-75, C-86, Wf-77 and W-88, which is absent for samples at a lower activation level. However, an increased activation gives the displacement of the $IPSD_V$ peaks of broad mesopores and macropores towards smaller x values (Fig. 2), and the V_{mac}/V_p value decreases (Fig. 1). This result can be explained by the origin of these pores, which have a textural character as voids between porous nanoparticles (see Figs.

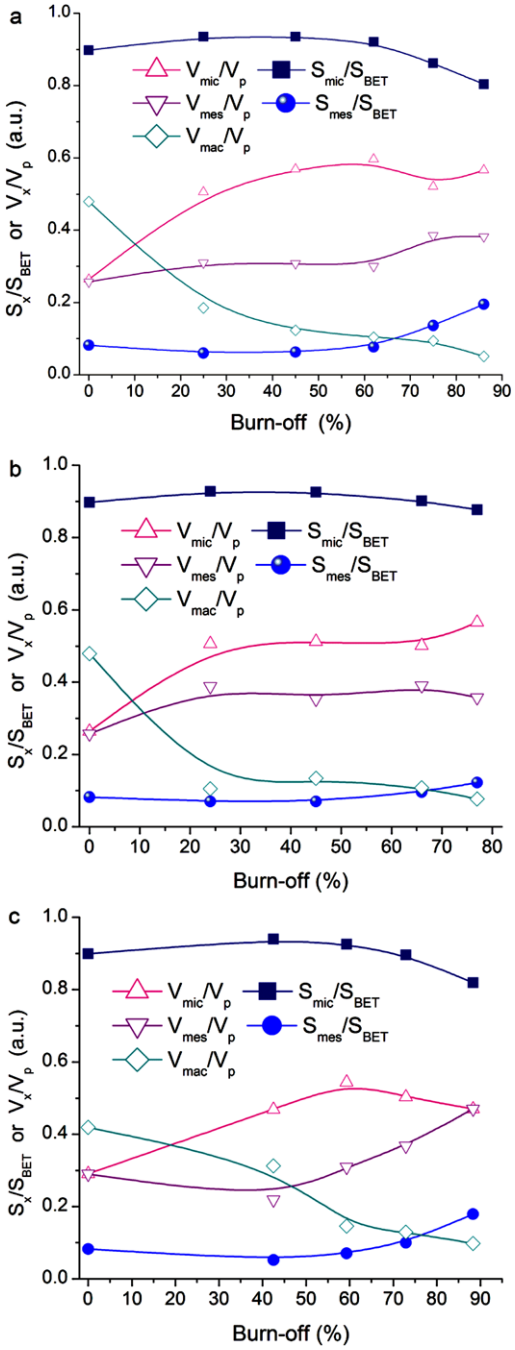

Fig. 1 Relationships between S_{mic}, S_{mes} and S_{BET} and V_{mic}, V_{mes}, V_{mac} and V_p for AC activated by (**a**) CO_2 and water vapour in (**b**) fixed and (**c**) fluidised bed reactors

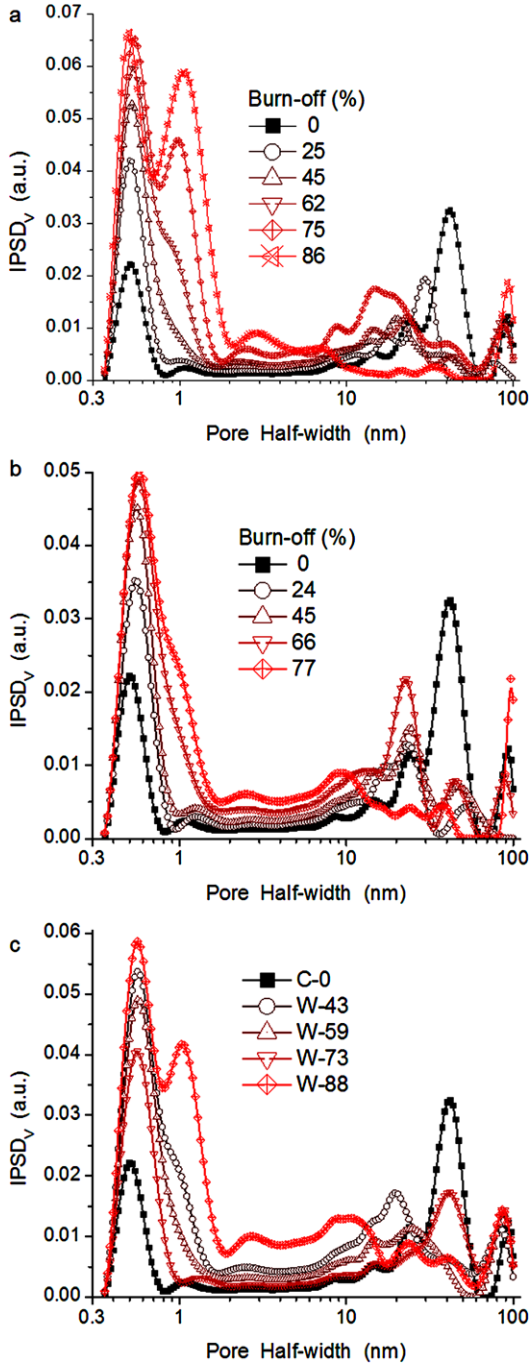

Fig. 2 Incremental PSD_V for carbon samples activated by (**a**) CO_2 and water vapour in (**b**) fixed and (**c**) fluidised bed reactors, DFT method with the model of slitshaped pores

S1 and S2 in Electronic supplementary material). The increased activation leads to diminution of the size of these nanoparticles, and voids between smaller particles become narrower. Water molecules as smaller than CO_2 molecules can penetrate into smaller pores and change their structure more strongly and add to the mesoporosity (even decreasing microporosity, Fig. 1c, V_{mic}/V_p) with respect to both pore volume (Fig. 2, C-86 and W-88) and specific surface area (Fig. 1, S_{mes}/S_{BET}). However, an increase in the activation from 62 to 86% burn-off does not practically increase overall contribution of the narrowest micropores, despite partial disruption of the pore walls and increasing contribution of narrow mesopores at $x < 2$ nm (Fig. 2a).

Notice that the relative contribution of micropores decreases (Fig. 1). The maximal activation with water vapour

Table 1 Structural characteristics of activated carbons (model of slit-like pores) activated by CO_2 (C-x samples) and water vapour (Wf-x and W-i samples)

Sample	S_{BET} m^2/g	S_{mic} m^2/g	S_{mes} m^2/g	S_{mac} m^2/g	V_p cm^3/g	V_{mic} cm^3/g	V_{mes} cm^3/g	V_{mac} cm^3/g	Δw
C-0	549	493	45	11	0.981	0.259	0.253	0.469	0.007
C-25	1082	1011	65	6	1.011	0.511	0.314	0.187	0.061
C-45	1615	1510	101	4	1.319	0.751	0.406	0.162	0.132
C-62	2270	2090	175	4	1.683	1.004	0.505	0.175	0.240
C-75	3047	2626	413	6	2.349	1.223	0.904	0.222	0.334
C-86	3463	2181	1279	3	2.320	1.314	0.887	0.119	0.304
C-86*	3463	1490	1969	4	2.320	0.606	1.567	0.148	0.626
C-30[a]	1145	1052	88	5	1.187	0.554	0.469	0.164	0.157
C-60	1999	1729	250	19	1.969	0.663	0.638	0.669	0.561
Wf-24	963	894	67	3	0.908	0.460	0.352	0.095	0.084
Wf-45	1194	1199	91	5	1.208	0.620	0.427	0.162	0.098
Wf-66	1780	1606	171	5	1.606	0.806	0.627	0.173	0.206
Wf-77	2080	1826	253	3	1.826	0.894	0.563	0.122	0.268
W-43	1189	1118	62	9	1.235	0.579	0.270	0.386	0.157
W-59	1677	1553	118	5	1.442	0.785	0.446	0.211	0.222
W-73	2069	1855	208	6	1.825	0.918	0.671	0.236	0.265
W-88	2793	2288	500	6	2.350	1.105	1.105	0.230	0.329
W-88*	2793	786	1989	19	2.350	0.544	1.458	0.348	0.588

Note. Contribution of micropores (S_{mic}, V_{mic}) at half-width $x < 1$ nm, mesopores (S_{mes}, V_{mes}) at $1 < x < 25$ nm, and macropores (S_{mac}, V_{mac}) at $x > 25$ nm; Δw is the relative deviation of the pore shape from the slitshaped model. *Model with a mixture of slitshaped (relative contribution 0.533 and 0.534 for C-86 and W-88, respectively) and cylindrical (0.335 and 0.363) pores and voids between spherical nanoparticles (0.132 and 0.103) calculated using the self-consisting regularisation procedure

[a]C-30 was catalytically activated

more strongly increases contribution of large mesopores than the activation with CO_2. However, the character of structural changes depends on the type of a reactor used and other conditions on activation by water vapour (comp. Figs. 2b and 2c, and series of Wf-x and W-x in Table 1). In the case of the fluidised bed reactor, contribution of narrow mesopores is larger than that for samples prepared in the fixed bed reactor. Notice that further activation of carbons at burn-off >86–88% was not carried out because of a low yield of AC.

The analysis of the SAXS data with respect to the structural characteristics of ACs (Fig. 3a and Fig. S3) shows that an increase in the burn-off level leads to the displacement of the PSD peaks of micro- and mesopores in the opposite directions similar to the effect observed in the PSDs calculated from the nitrogen adsorption data (Fig. 2). Both types of the PSDs are in good agreement for ACs with different burn-off (Fig. S3) despite the difference in the methods and the pore models used. Consequently, the main details of the PSDs depend more strongly on the type of ACs than on the pore models used on treatment of the nitrogen adsorption and SAXS data. However, the PSDs calculated using the different pore models for the nitrogen adsorption have the shapes with a systematic displacement of the peaks and model-dependent intensity (Fig. S4).

For the AC pore walls, small chord lengths (mainly < 2 nm) are characteristic (Fig. 3b), whose contribution increases with increasing burn-off. This suggests that the AC walls are thin (~1 nm corresponding to stacks with two-three carbon sheets) with a rough surface and become thinner and rougher with increasing activation. This assumption is in agreement with the analysis of the structural features of ACs based on the PSDs (Fig. 2), relative changes in micro- and mesoporosity (Fig. 1), and increased deviations of the pore shapes from the models as a measure of the surface roughness (Table 1, Δw).

Smaller Δw values (Table 1) are observed at lower burn-off value, and the minimal Δw value is for AC at the lowest S_{BET} value. The activation of ACs by CO_2 and water vapour gives close changes and tendencies in these changes in the AC structure (Figs. 1 and 2). However, the activation with H_2O in the fluidised bed reactor gives slightly greater deviations in the pore shape from the model of slitshaped pores than the activation with CO_2 or water vapour in the fixed bed reactor (Table 1, Δw). This result can be explained by stronger effects of the wa-

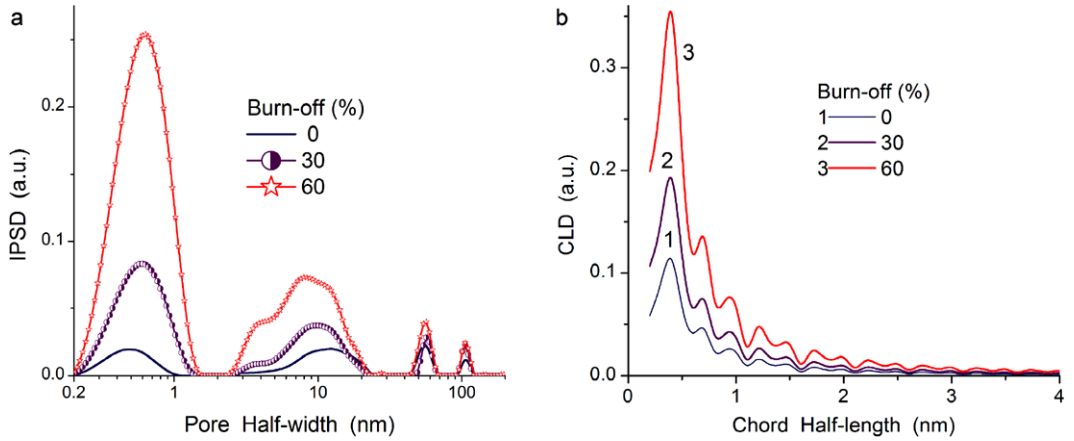

Fig. 3 Pore size (**a**) and chord length, CLD (**b**) distributions for ACs at different burn-off levels calculated from the SAXS data; the specific surface area $S_{SAXS} = 610$, 1080, and 1811 m^2/g, respectively

ter vapour flow on narrow slitshaped pores than on textural pores as voids between carbon nanoparticles composing carbon granules of 0.1–0.5 mm in size (Figs. S1 and S2). Since the IPSD intensity at $x > 20$ nm is higher for the CO_2-activated samples (Fig. 2a) than that for the H_2O-activated ACs (Fig. 2c). The maximal deviations in the pore shape from the slitshaped model are observed for C-86 and W-88 (Table 1). One can assume that the maximal crumpling of single-double carbon sheets is for C-86. There are not stacks with many carbon sheets since $S_{BET} > 3400$ m^2/g (at a small BET constant $c_{BET} = 50.3$). The self-consisting regularisation with the mixture of different pore models gives close contributions of pores of different shapes for C-86 and W-88 (see Note in Table 1). This is due to a close shape of their PSDs at $x < 2$ nm (Fig. 2) at contribution of slitshaped pores of 53% for both samples.

All the studied ACs are characterised by broad PSD_V (Fig. 2) with significant contributions of micro-, meso- and macropores (Table 1). However, narrow slitshaped pores at $x < 2$ nm give the maximal contribution since $S_{mic}/S_{BET} > S_{mes}/S_{BET}$ and $V_{mic}/V_p > V_{mes}/V_p$ (Fig. 1). Materials with similar structural characteristics can be effective adsorbents for small molecules (Marsh et al. 1997; Silvestre-Albero et al. 2010; Bansal et al. 1988) because significant adsorption is possible if the pore size smaller than four times diameter of the adsorbate molecules.

To study the interfacial behaviour of different adsorbates with a small size of the molecules (e.g. H_2, CH_4, etc.), carbon C-30 was chosen as a representative sample with relatively small contribution of broad pores to the specific surface area since $(S_{mes} + S_{mac})/S_{BET} = 0.081$ (Table 1), broad PSD, low contribution of narrow mesopores (Fig. S4b) and V_{mic} close to $V_{mes} + V_{mac}$. Notice that broad pores are not appropriate for adsorption of small molecules of the probes studied.

Water adsorbed in textural broad voids and narrow pores in C-30 is characterised by two signals in the ^1H NMR spectra (Fig. 4a).

However, these signals do not split because of the large amount of adsorbed water (75 wt%) and the existence of fast molecular exchange between water structures located in different pores. Water in broad pores is weakly bound, and therefore it is completely frozen at $T < 265$ K (Fig. 4a) since signal 2 disappears at $T < 265$ K. Water in narrow slitshaped pores is unfrozen even at 200 K (Fig. 4a, signal 1) and characterised by the signal shifted towards the strong magnetic field because of the shielding effects of the π-electron current at the basal planes that increase in narrower pores. Additionally, the ^1H NMR signals of adsorbed water shift towards the strong magnetic field with lowering temperature because water freezes in narrower pores (where the shielding effect of the π-electrons is stronger) at lower temperatures (Gun'ko et al. 2005; Krutyeva et al. 2009) due to stronger freezing point depression for liquids confined in narrower pores.

Co-adsorption of water and chloroform-d results in the displacement of water by weakly polar (hydrophobic) chloroform from narrow pores. Therefore all water is completely frozen at $T < 260$ K (Fig. 4b) that suggests that all displaced water is weakly bound and located in broad pores (i.e. in textural voids between carbon nanoparticles) or on the outside of carbon granules (Gun'ko et al. 2005). Notice that the signal of displaced water is at $\delta_H = 5$ ppm (typical value for bulk water with high associativity of the molecules) which is greater than $\delta_H = 3$ ppm without chloroform-d, i.e. water associativity increases due to interaction with chloroform. This can be caused by displacement of water into larger pores or out of them where the associativity of water molecules can increase.

On the adsorption of methane and hydrogen, a rubber reservoir with a gas (pressure 1.1 atm) was connected to

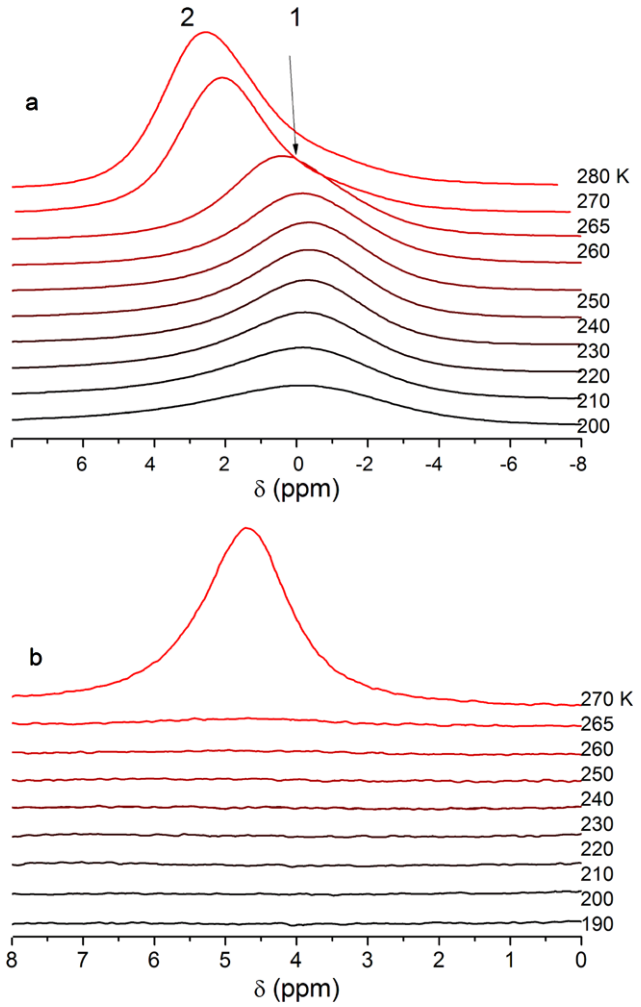

Fig. 4 ^{1}H NMR spectra of water (0.75 g per gram of dry carbon) adsorbed on C-30 at different temperatures and different media: (**a**) air and (**b**) chloroform-d

a NMR ampoule. Therefore, the adsorbed amounts of CH_4 or H_2 can increase with lowering temperature (Figs. 5a and 5b). For both methane and hydrogen, the displacement of the ^{1}H NMR signal towards the strong magnetic field is observed since for free gases $\delta_H \approx 0$ and 4 ppm, respectively. In contrast to CH_4 (Fig. 5a) the H_2 adsorption is very small (Fig. 5b) because C-30 is not a pure microporous carbon and has a broad PSD (Figs. 3a and S4b). In contrast to water (Fig. 4a), adsorbed methane is characterised by the ^{1}H NMR signal shifted towards the weak magnetic field with lowering temperature (Fig. 5a) because it is unfrozen (freezing temperature $T_f = 90.7$ K) over the total range of used temperatures and its adsorption increases ($p = 1.1$ atm in the CH_4 reservoir) in larger pores with the reduced shielding effect with decreasing temperature.

On the adsorption of chloroform-H, four ^{1}H NMR signals are observed at $\delta_H = 0.5$, 3.5–3, 4.5–5 and 7.2 ppm at $T > 210$ K (Fig. 5c). The intensity of signals 3 and 4 strongly decreases at $T < 210$ K since freezing temperature of $CHCl_3$ is $T_f = 209.7$ K. Therefore, these signals can be assigned to chloroform-H located in broad pores or out of pores. Signal 4 at 7.2 ppm corresponds to practically free liquid (e.g. adsorbed in macropores, Fig. S4b) but signal 3 at 4.5–5 ppm can be due to chloroform located in broad mesopores. Signals 1 and 2 are due to the adsorption of chloroform in narrow mesopores and micropores. Thus, the lower the δ_H value, the narrower are the pores where the $CHCl_3$ molecules are located. The signal of chloroform located in the narrowest pores (Fig. S4b, $x < 1$ nm) does not diminish at lower temperatures in contrast to that of molecules located in broader pores because of stronger freezing point depression for adsorbates confined in narrower pores.

The freezing effect is not observed for CH_2Cl_2 (Fig. 5d) because its $T_f = 176.2$ K is lower than the temperature range used. A decrease in the signal at 2 ppm with lowering temperature can be due to the formation of larger Van der Waals clusters in larger pores with decreasing temperature. A similar but stronger effect is also observed for the CH_2Cl_2-DMSO-d_6 mixture (Fig. 5e) due to stronger rearrangement of this mixture with lowering temperature. This can be due to large differences in the T_f values (~115 K), polarity (donor number ~0 and 125 kJ/mol, respectively), interaction energy with AC and molecular sizes of co-adsorbates. Similar effects were observed for different adsorbents (Gun'ko et al. 2005), and a similar effect of 'freezing' of the signal in the strong magnetic field is observed for the H_2–H_2O mixture (Fig. 5f). Thus, this phenomenon reflects certain regularities in the interfacial behaviour of the mixtures with compounds unfrozen and frozen in a given temperature range due to, at least, reasons: (i) variations in the freezing point depression for different liquids confined in different pores, (ii) diminution of the mobility of small molecules with decreasing temperature that allows them to be adsorbed in larger pores, and (iii) a frozen phase (or an immobilise phase) can change the topology of pores filled by an unfrozen phase. Therefore, the adsorption of H_2 or CH_4 onto different adsorbents can increase due to pre-adsorption of water or other adsorbates with relatively high T_f values (Gun'ko et al. 2008a, 2008b). Another important factor is the affinity of the AC surface with respect to one of adsorbates that can be changed due to surface modification (e.g. oxidation, grafting functionalities with H, N, S, P and other atoms). Uniform or non-uniform modification can affect adsorption of a given adsorbate in the form of films (completely filling narrow pores) or clusters (e.g. at the edges of carbon sheets).

4 Conclusion

Activated carbons prepared with the same precursor but differently activated by CO_2 or water vapour demonstrate

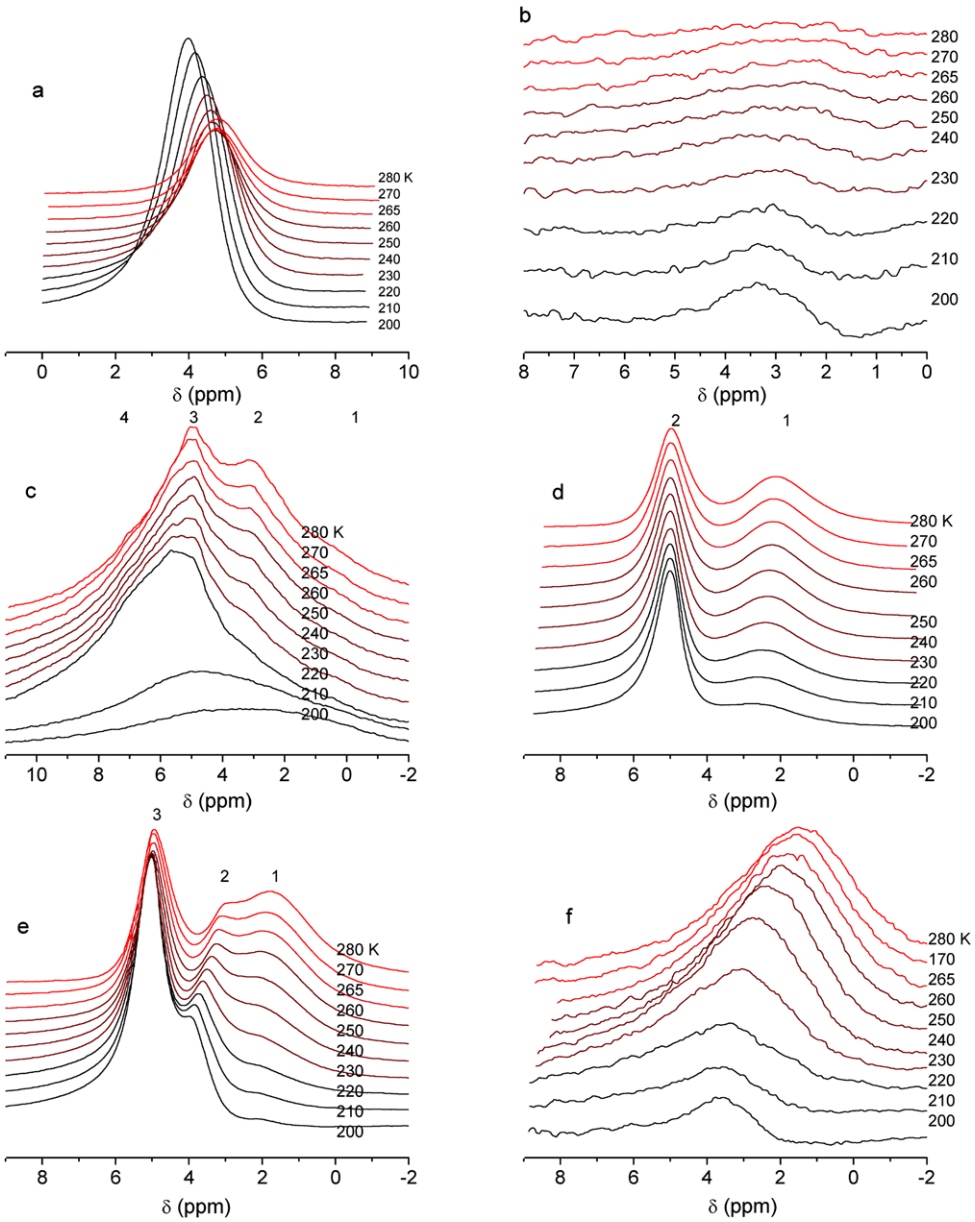

Fig. 5 ^{1}H NMR spectra of (**a**) CH_4 (freezing point $T_f = 90.7$ K), (**b**) H_2 ($T_f = 14$ K), (**c**) $CHCl_3$ ($T_f = 209.7$ K), (**d**) CH_2Cl_2 ($T_f = 176.2$ K), (**e**) CH_2Cl_2 + DMSO-d_6 (40 wt% pre-adsorbed, $T_f = 291.6$ K), (**f**) $H_2 + H_2O$ (2 wt% pre-adsorbed)

increased deviation of the pore shape from the slitshaped model with increasing contribution from pores over a broad range with increasing burn-off. This occurs due to enhanced crumpling of single sheets or stacks with a small number of sheets and reduction of the sizes on nanoparticles (formed with these crumpled sheets) packed in carbon globules with increasing activation. Activation by both CO_2 and water vapour results in close changes in contributions of micro-, meso- and macropores depending on burn-off, and contribution of macropores decreases in contract to mesoporosity. Relative contribution of micropores to the specific surface area decreases with increasing burn-off. Changes in the mesoporosity have a more complex character because tendency in changes of narrow mesopores (close in size to micropores) can differ from that for broad mesopores (close in size to macropores).

The interfacial behaviour of different adsorbates adsorbed alone or in various mixtures on AC depends strongly on temperature, especially when current temperature becomes lower than freezing temperature of one of the adsorbed compounds. Significant re-arrangement of adsorption complexes, especially of the Van der Waals type characteristic for nonpolar or weakly polar adsorbates, occurs in both micropores and mesopores with decreasing temperature. The temperature behaviour of the mixtures can strongly differ from that of individual adsorbates. These effects should be considered in practical applications of activated carbons for adsorption of various mixtures at different, especially low, temperatures.

Acknowledgements The work was supported in part by grants under the Seventh Framework Programme (FP7/2007-2013), Marie Curie International Research Staff Exchange Scheme (grant no. 230790 and 247547) and Marie-Curie Industry-Academia Partnerships and Pathways Agreement (PIAP-GA-2008-218242). V.M.G. and V.V.T. are grateful to the STCU (grant no. 4481). The authors are grateful to the ESRF, Grenoble, for access to the French CRG beamline D2AM and they acknowledge the help of its technical staff, Jean-François Berar, Nathalie Boudet, Bernard Caillot, Stephan Arnaud, and Dr. J.I. Paredes (Instituto del Carbon, Oviedo, Spain) for the help in AFM study of AC.

References

Ahumada, E., Lizama, H., Orellana, F., Suárez, C., Huidobro, A., Sepúlveda-Escribano, A., Rodríguez-Reinoso, F.: Catalytic oxidation of Fe(II) by activated carbon in the presence of oxygen. Effect of the surface oxidation degree on the catalytic activity. Carbon **40**, 2827–2834 (2002)

Bansal, R.C., Donnet, J.B., Stoeckli, F.: Active Carbon. Marcel Dekker, New York (1988)

Dieudonné, Ph., Hafidi Alaoui, A., Delord, P., Phalippou, J.: Transformation of nanostructure of silica gels during drying. J. Non-Cryst. Solids **262**, 155–161 (2000)

Do, D.D., Nguyen, C., Do, H.D.: Characterization of micromesoporous carbon media. Colloids Surf. A **187–188**, 51–71 (2001)

Gregg, S.J., Sing, K.S.W.: Adsorption, Surface Area and Porosity, 2nd edn. Academic Press, San Diego (1982)

Gun'ko, V.M.: Consideration of the multicomponent nature of adsorbents during analysis of their structural and energy parameters. Theor. Exp. Chem. **36**, 319–324 (2000)

Gun'ko, V.M., Do, D.D.: Characterization of pore structure of carbon adsorbents using regularization procedure. Colloids Surf. A **193**, 71–83 (2001)

Gun'ko, V.M., Mikhalovsky, S.V.: Evaluation of slitlike porosity of carbon adsorbents. Carbon **42**, 843–849 (2004)

Gun'ko, V.M., Turov, V.V., Bogatyrev, V.M., Zarko, V.I., Leboda, R., Goncharuk, E.V., Novza, A.A., Turov, A.V., Chuiko, A.A.: Unusual properties of water at hydrophilic/hydrophobic interfaces. Adv. Colloid Interface Sci. **118**, 125–172 (2005)

Gun'ko, V.M., Kozynchenko, O.P., Turov, V.V., Tennison, S.R., Zarko, V.I., Nychiporuk, Y.M., Kulik, T.V., Palyanytsya, B.B., Osovskii, V.D., Ptushinskii, Y.G., Turov, V.A.: Structural and adsorption characteristics of activated carbons possessing significant textural porosity. Colloids Surf. A **317**, 377–387 (2008a)

Gun'ko, V.M., Turov, V.V., Kozynchenko, O.P., Palijczuk, D., Szmigielski, R., Kerus, S.V., Gorbik, P.P.: Characteristics of adsorption phase with water/organic mixtures at a surface of activated carbons possessing intraparticle and textural porosities. Appl. Surf. Sci. **254**, 3220–3231 (2008b)

Juárez-Galán, J.M., Silvestre-Albero, A., Silvestre-Albero, J., Rodríguez-Reinoso, F.: Synthesis of activated carbon with highly developed "mesoporosity". Micropor. Mesopor. Mater. **117**, 519–521 (2009)

Krutyeva, M., Grinberg, F., Furtado, F., Galvosas, P., Kärger, J., Silvestre-Albero, A., Sepulveda-Escribano, A., Silvestre-Albero, J., Rodríguez-Reinoso, F.: Characterization of carbon materials with the help of NMR methods. Micropor. Mesopor. Mater. **120**, 91–97 (2009)

Lenghaus, K., GuangHua Qiao, G., Solomon, D.H., Gomez, C., Rodríguez-Reinoso, F., Sepulveda-Escribano, A.: Controlling carbon microporosity: the structure of carbons obtained from different phenolic resin precursors. Carbon **40**, 743–749 (2002)

Marsh, H., Heintz, E.A., Rodriguez-Reinoso, F. (eds.): Introduction to Carbon Technologies. University of Alicante, San Vicente del Raspeig (1997)

Molina-Sabio, M., Rodríguez-Reinoso, F.: Role of chemical activation in the development of carbon porosity. Colloids Surf. A **241**, 15–25 (2004)

Molina-Sabio, M., Rodríguez-Reinoso, F., Caturla, F., Sellés, M.J.: Porosity in granular carbons activated with phosphoric acid. Carbon **33**, 1105–1113 (1995)

Molina-Sabio, M., Rodríguez-Reinoso, F., Caturla, F., Sellés, M.J.: Development of porosity in combined phosphoric acid-carbon dioxide activation. Carbon **34**, 457–462 (1996)

Provencher, S.W.: A constrained regularization method for inverting data represented by linear algebraic or integral equations. Comput. Phys. Commun. **27**, 213–227 (1982)

Pujari, P.K., Sen, D., Amarendra, G., Abhaya, S., Pandey, A.K., Dutta, D., Mazumder, S.: Study of pore structure in grafted polymer membranes using slow positron beam and small-angle X-ray scattering techniques. Nucl. Instrum. Methods Phys. Res. B **254**, 278–282 (2007)

Rodríguez-Reinoso, F.: The role of carbon materials in heterogeneous catalysis. Carbon **36**, 159–175 (1998)

Rodriguez-Reinoso, F.: Porous carbons in gas separation and storage. In: Loureiro, J.M., Kartel, M.T. (eds.) Combined and Hybrid Adsorbents, Fundamentals and Applications. NATO Security through Science Series C: Environmental Security, pp. 133–144. Springer, Dordrecht (2006)

Rodríguez-Reinoso, F., Molina-Sabio, M., González, M.T.: The use of steam and CO_2 as activating agents in the preparation of activated carbons. Carbon **33**, 15–23 (1995)

Rodríguez-Reinoso, F., Pastor, A.C., Marsh, H., Martínez, M.A.: Preparation of activated carbon cloths from viscous rayon. Part II: physical activation processes. Carbon **38**, 379–395 (2000a)

Rodríguez-Reinoso, F., Pastor, A.C., Marsh, H., Huidobro, A.: Preparation of activated carbon cloths from viscous rayon. Part III: effect of carbonization on CO_2 activation. Carbon **38**, 397–406 (2000b)

Sarnatskaya, V.V., Lindup, W.E., Walter, P., Maslenny, V.N., Yushko, L.A., Sidorenko, A.S., Nikolaev, A.V., Nikolaev, V.G.: Albumin, bilirubin, and activated carbon: new edges of an old triangle. J. Art. Cells, Blood Subs. Immob. Biotech. **30**, 113–126 (2002)

Sarnatskaya, V.V., Yushko, L.A., Nikolaev, A.V., Grinenko, D.V., Nikolaev, V.G.: New approaches to the removal of protein-bound toxins from blood plasma of uremic patients. Biomater. Artif. Cells Artif. Organs **35**, 287–309 (2007)

Silvestre-Albero, A., Ramos-Fernández, J.M., Martínez-Escandell, M., Sepúlveda-Escribano, A., Silvestre-Albero, J., Rodríguez-Reinoso, F.: High saturation capacity of activated carbons prepared from mesophase pitch in the removal of volatile organic compounds. Carbon **48**, 548–556 (2010)

Smisek, M., Cerny, S.: Active Carbon. Elsevier, Amsterdam (1970)

Tennison, S.R., Kozynchenko, O.P., Strelko, V.V., Blackburn, A.J.: Porous carbons, US Patent 2004, 024,074A1 (2004)